How to cite: *Angew. Chem. Int. Ed.* **2023**, *62*, e202303083
doi.org/10.1002/anie.202303083

Non-innocent Ligands

Hydrocarbon Oxidation by a Porphyrin-π-Cation Radical Complex

*Marta Lovisari, Oscar Reid Kelly, and Aidan R. McDonald**

Abstract: Heme and chlorin π-cation radical oxidants are widely implicated in biological and synthetic oxidation catalysis. Little insight into the role of π-cation radicals in proton coupled electron transfer (PCET) oxidation is available. We prepared a Ni^{II}-porphyrin-π-cation complex ($[Ni^{II}(P^{\bullet+})]$) and found it to be capable of the oxidation of a variety of simple hydrocarbon substrates. Interestingly, some of the products were hydroxylated, with ($[Ni^{II}(P^{\bullet+})]$) working in concert with atmospheric O_2 to yield hydroxylated hydrocarbons. Kinetic data suggested that the porphyrin-π-cation radical species oxidised substrates through a concerted PCET mechanism, where the porphyrin-π-cation radical accepted the electron, and the proton was transferred to a free anion. Our findings highlight the potential role of π-cation radicals as hydrocarbon activators, demonstrating that porphyrin ligand non-innocence could be a readily manipulated resource for oxidation catalyst development.

Introduction

Heme- and chlorin-based oxidants are implicated in a variety of oxidative transformations.[1] Compound I, an $O{=}Fe^{IV}$-porphyrin-π-cation radical complex, is the active oxidant in heme-containing cytochrome P450 oxidases, heme-halogenases, and haloperoxidases.[1c,g] Compound I has been shown to perform a proton coupled electron transfer (PCET) oxidation where the oxo-ligand acts to abstract a hydrogen atom from a hydrocarbon substrate, yielding compound II, an $H{-}O{-}Fe^{IV}$-porphyrin complex.[2] In this case, the porphyrin-π-cation radical ultimately accepts the electron from the PCET event. $P680^+$, the primary electron donor in photosystem II (PSII),[1a,d] is a postulated chlorin-π-cation radical complex (formed from chlorophyll) purported to drive water oxidation at the oxygen evolving complex in PSII. $P680^+$ has been identified as the most powerful oxidant in nature, displaying a redox potential of approximately 1.2 V versus the standard hydrogen electrode (SHE).[1a,d,3] $P680^+$ is postulated to perform PCET oxidation of a neighbouring tyrosine O–H group, where the chlorin-π-cation radical acts to accept the electron, yielding chlorophyll. π-Cation radical species thus represent a class of powerful biological oxidants involved in important PCET oxidation reactions.

Many examples of synthetic metal-based oxidants and oxidation catalysts supported by porphyrin and porphyrinoid ligands have been reported.[4] As with the heme examples described above, these systems all focussed on reactions involving metal-dioxygen, -peroxide, -oxide, and -hydroxide adducts, where the oxygen ligands act as proton acceptors in PCET oxidation reactions, mimicking the heme paradigm. Recent efforts have expanded our understanding of high-valent oxidants, showing that other ancillary ligands (N, Cl, F) can act as the proton acceptors in PCET oxidations.[5] The role of the π-cation radical in PCET has been largely ignored, apart from investigations into its influence on the reactivity on a terminal M=O entity.[4f,6] This is despite the ubiquity of porphyrinoid π-cation radical species in biological and synthetic oxidation reactions. To the best of our knowledge, there are no studies into the capabilities of just the π-cation radical complex in PCET oxidation reactions.

Results and Discussion

The free-base porphyrin $H_2T(MeO)PP$ (*meso*-tetra(4-methoxyphenyl)porphyrin) was synthesized according to a literature procedure.[7] In order to probe *just* the role of the π-cation radical in PCET, we selected four-coordinate nickel-porphyrin complexes that are stable *without* ancillary, potentially proton accepting, ligands. Four-coordinate Fe-porphyrin complexes are extremely rare and thus inaccessible.[8] The synthesis of the Ni^{II} complex, $[Ni^{II}(T(MeO)PP)]$ (**1**) was performed by refluxing the free base $H_2T(MeO)PP$ with an excess of $NiCl_2{\cdot}6H_2O$ (3 equiv) in *N*,*N*-dimethylformamide (DMF, see Supporting Information for details). The ^1H NMR spectrum of **1** showed resonances consistent with complexation (Figure S1).[9] Electro-spray ionization mass spectrometry (ESI-MS) showed the presence of a peak at $m/z = 791.2172$ assigned to the $[\mathbf{1}{+}H]^+$ cation (expected $m/z = 791.2163$, Figure S2). The electronic absorption spectrum of **1** showed an intense Soret band at $\lambda = 428$ nm and a second absorption band at $\lambda = 530$ nm (Figure 1). Cyclic voltammetry on **1** showed redox properties typical of Ni^{II}-porphyrin complexes (Figure S3).[10] Two reversible redox waves were observed at $E_{1/2} = 0.54$ and 0.85 V versus ferrocene/ferrocenium (Fc/Fc^+), which were

[*] M. Lovisari, O. Reid Kelly, A. R. McDonald
School of Chemistry, Trinity College Dublin, the University of Dublin
College Green, Dublin 2 Dublin 2 (Ireland)
E-mail: aidan.mcdonald@tcd.ie

assigned to the (formally) Ni^{II}/Ni^{III} and Ni^{III}/Ni^{IV} couples, respectively, with the recognition that the oxidations may be borne by the porphyrin ligand rather than Ni.

The chemical oxidation **1** at 20 °C (Scheme 1), with an excess (2 equiv) of the one-electron oxidants phenoxathiinyl hexachloroantimonate ((Phenox)$SbCl_6$), *tris*-(4-bromophenyl)ammoniumyl hexachloroantimonate (magic blue), or WCl_6 (0.70–1.36 V vs Fc/Fc^+),[11] resulted in the formation of a new species (**2**) according to electronic absorption spectroscopy (Figures 1, S4, S5). The starting red solution of **1** turned a deep green colour for **2** (a putative Ni^{II}-porphyrin-π-cation radical complex). The highest yield was obtained when (Phenox)$SbCl_6$ was employed as an oxidant. A spectroscopically monitored titration of (Phenox)$SbCl_6$ with **1** was performed, showing that the maximum yield of **2** was reached when approximately 1.5 equivalents of oxidant were added (Figure 1). As the conversion of **1** into **2** should be a 1-electron conversion, we attribute the need for more-than-one equivalent of (Phenox)$SbCl_6$ to its poor stability (it decays rapidly in solution and even in the solid-state).

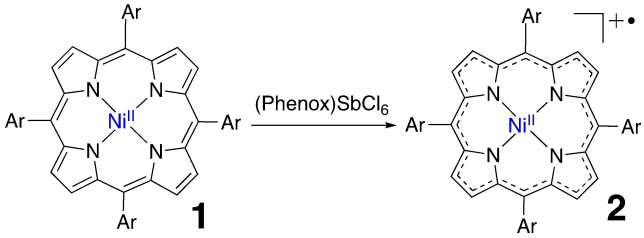

Scheme 1. Complex **1** and its conversion into **2**. Phenox = phenoxathiinyl radical cation; Ar = 4-methoxyphenyl.

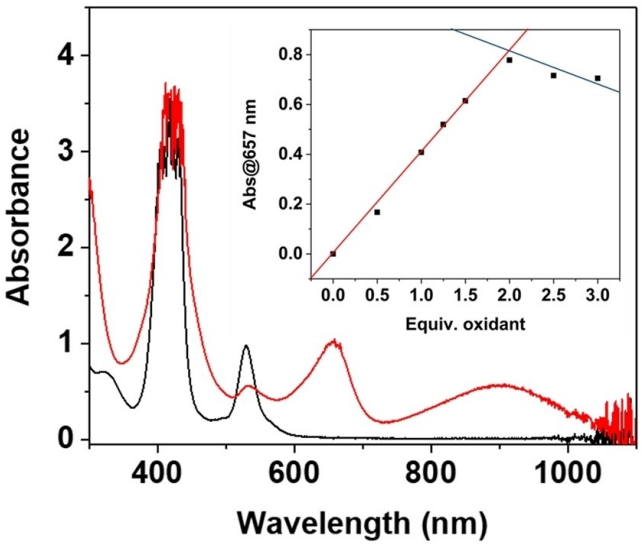

Figure 1. Electronic absorption spectra of **1** (0.085 mM, CH_2Cl_2, 20 °C, black trace) and **2** (red trace, after the addition of (Phenox)$SbCl_6$ (2 equiv) to **1**). Inset: titration of (Phenox)$SbCl_6$ with **1** (20 °C, CH_2Cl_2), monitoring at $\lambda = 657$ nm.

2 displayed a change in the Q-band region of the electronic absorption spectrum when compared to **1**, with new absorption bands at $\lambda_{max} = 657$, 900 nm. Absorptions between $\lambda = 600$–700 nm have been attributed to the formation of other Ni^{II}-porphyrin-π-cation radical species ($[Ni^{II}(P^{\bullet+})]$, P = porphyrin).[12] In contrast, a less significant shift in the Q bands and a sharp peak at $\lambda = 570$ nm has been attributed to $[Ni^{III}(P)]^+$ species, where the metal has borne the oxidation. The presence and the intensity of the near-IR feature at $\lambda_{max} = 900$ nm is comparable to some $[Ni^{II}(P^{\bullet+})]$ species. For example, it was absent for $[Ni^{II}(TPP^{\bullet+})]$ (TPP = tetraphenylporphyrin) but present for the more flexible $[Ni^{II}(OEP^{\bullet+})]$ (OEP = octaethylporphyrin), which showed an absorption band at $\lambda = 911$ nm.[13] The presence of electronic absorption features typical of those attributed to porphyrin-π-radical cation species led us to conclude that **2** be described as a Ni^{II}-porphyrin-π-radical cation, $[Ni^{II}(T(MeO)PP^{\bullet+})]$.

The Fourier transform infrared (FTIR) spectrum of **2** showed an intense and sharp feature at $\nu = 1263\ cm^{-1}$ which was not present in the spectrum of **1** (Figure S6). Sharp bands in the region between 1250 and 1295 cm^{-1} are diagnostic of a porphyrin-based oxidation in metalloporphyrins.[14] This band was ascribed to a ring vibrational mode typical of porphyrin-π-radical cations in tetra-arylporphyrin complexes. ESI-MS showed the presence of a peak at $m/z = 790.2040$ assigned to the Ni-porphyrin-cation radical ($\{[Ni^{II}(T(MeO)PP^{\bullet+})]\}^+$ expected $m/z = 790.2090$, Figure S7), consistent with our assignment of **2** as $[Ni^{II}(T(MeO)PP^{\bullet+})]$. This cation was not observed in the mass spectrum of **1**, which only showed the $[\mathbf{1}+H]^+$ cation ($m/z = 791.2172$, Figure S2). These results corroborated our assignment of **2** as $[Ni^{II}(T(MeO)PP^{\bullet+})]$.

An X-band EPR spectrum of **2** showed an isotropic signal at g = 2.00, indicative of an $S = {}^1/_2$ organic radical species (Figure 2). The EPR spectrum of the starting material **1** was EPR silent, as expected for a square-planar Ni^{II} complex. We therefore ascribed the observed signal for **2** to a one-electron oxidised species, where the oxidation was borne by the ligand to yield a porphyrin-π-radical cation species $[Ni^{II}(T(MeO)PP^{\bullet+})]$. For such complexes, valence tautomerism has been observed. For example, $[Ni^{II}(TPP^{\bullet+})]$ displayed an isotropic EPR signal at g = 2.00 at 295 K, indicative of porphyrin oxidation. When frozen at 77 K, the same sample yielded an anisotropic EPR signal indicative of an isomerization to $[Ni^{III}(TPP)]$.[15] The EPR properties of **2** were also probed when WCl_6 was used in its preparation. WCl_6 is EPR silent and when reduced to W^V (upon involvement in an oxidation reaction), it forms a dimer, W_2Cl_{10}, which is also EPR silent.[16] When we prepared **2** using WCl_6, the same isotropic signal at g = 2.00 was observed by EPR, confirming the assignment of the g = 2.00 signal to a porphyrin-π-cation radical and not (Phenox)$SbCl_6$ (Figure S8).

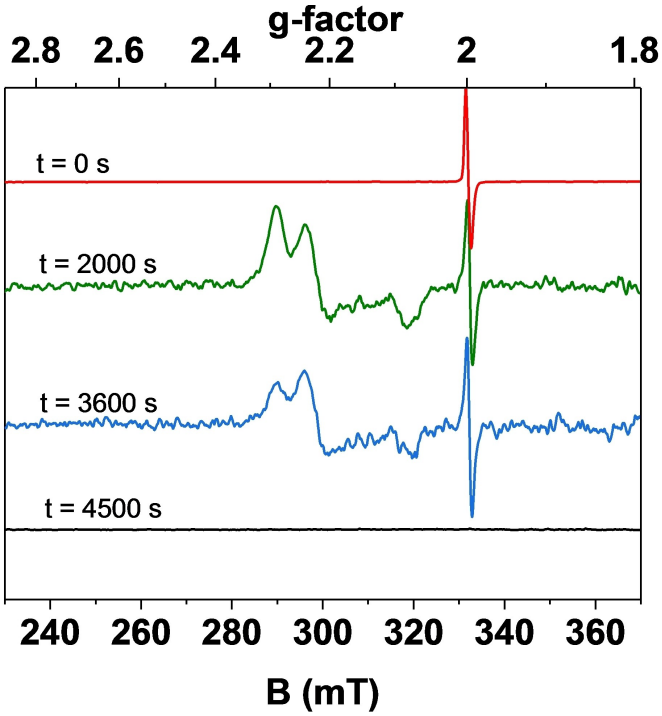

Figure 2. X-band EPR spectra of **2** (red trace) and its reaction with DHA (1500 equiv) after 2000 s (green trace), after 3600 s (blue trace) and after 4500 s (black trace) from the addition of the substrate. The spectra were acquired from CH_2Cl_2 solutions frozen at the given timepoint, 1.95 mW microwave power, 0.5 mT field modulation amplitude.

PCET Reactivity Properties of 2

The half-life of **2** was determined to be $t_{1/2}=3.5$ h at room temperature (20 °C), making the oxidised species sufficiently long-lived to perform detailed reactivity studies. **2** was reacted with 9,10-dihydroanthracene (DHA) under *pseudo*-first order conditions showing a relatively fast decay of the bands at $\lambda=657$, 900 nm by electronic absorption spectroscopy (Figure S9). Gas chromatographic (GC) and ^{1}H NMR (Figure S10) analysis of the post-reaction mixture showed anthracene had formed in approximately 65 % yield. Under aerobic conditions the yield was 150 %, showing that the substrate likely underwent auto-oxidation once exposed to **2** in an aerobic atmosphere. If **2** was a one electron oxidant, the maximum yield of anthracene would be 50 %, because the DHA to anthracene conversion is a two-electron (net two H-atoms transferred) process. We surmise that in the absence of air we observed quantitative conversion of DHA into anthracene (ca. 50 % yield, Table 1), and under aerobic conditions, once the radical is formed, auto-oxidation results in higher yields of anthracene (>150 %).

The formation of anthracene was further confirmed by optical spectroscopy ($\lambda=341$, 360 and 379 nm). The decay of the feature at $\lambda=657$ nm was fitted exponentially to obtain k_{obs} values at differing [DHA], which were then plotted against [DHA]. A linear trend was observed and from the slope of the plot we could obtain a second-order reaction rate constant, $k_2=0.019\ M^{-1}s^{-1}$ (Table 1). Compared to other oxidants capable of DHA oxidation at 20 °C, the obtained k_2 value was modest (*e.g.*, MnO_4^-: $^{DHA}k_2=0.12\ M^{-1}s^{-1}$).[17] Interestingly, the rate constant obtained under anaerobic conditions was comparable ($k_2=0.011\ M^{-1}s^{-1}$), demonstrating that atmospheric O_2 does not impact the rate of oxidation by **2**, which was thus capable of hydrocarbon activation yielding an oxidatively desaturated product.

Species **2** also reacted with xanthene, 1,4-cyclohexadiene (CHD), fluorene, and triphenylmethane, showing a decay of the features at $\lambda=657$, 900 nm upon addition to **2** in greater than 25-fold excess (Table 1, Figures S11–S14). All of the listed substrates displayed linear trends in the comparison of their measured k_{obs} against [substrate], yielding k_2 values. Substrates with C–H bonds stronger than those in triphenylmethane did not react with **2** (e.g., toluene). Species **2** was thus capable of reacting with substrates with relatively weak C–H bonds.

Xanthone was identified as the product of oxidation of xanthene by **2** using GC. Xanthone is a formally 4-electron oxidised product with an O-atom incorporated. Under anaerobic conditions, xanthone was not detected by GC analysis. ^{1}H NMR analysis of the CHD post-reaction mixture showed the formation of benzene, a formally 2-proton, 2-electron oxidation product of CHD (Figure S15). Benzene was obtained in 72 % yield, higher than the maximum 50 % conversion level. For the reaction with fluorene, we identified the oxygenated product 9-fluorenone as the major product by GC in 92 % yield. The oxidation of triphenylmethane produced the oxygenated product triphenylmethanol in 100 % yield, with respect to [**1**], according to GC analysis. For xanthene, fluorene, and triphenylmethane,

Table 1: k_2 values and yields of oxidation products from the reactions of **2** with different hydrocarbon substrates (CH_2Cl_2, 20 °C).

Substrate	k_2 [$M^{-1}s^{-1}$]	BDFE [kcal mol^{-1}]	Product	Yield [%][a]
xanthene	0.29	73.3	xanthone[c]	106 ± 4
CHD	0.026	*75.8*[b]	benzene[d]	72 ± 8
DHA	0.019	76.1	anthracene[c]	65 ± 5
fluorene	0.0086	77.4	9-fluorenone[c]	92 ± 6
triphenylmethane	0.0073	78.8	triphenylmethanol[c]	95 ± 5

[a] Yields were calculated with respect to the initial concentration of **1**. We assume that **2** acts as a one-electron oxidant. [b] A BDFE value for CHD in DMSO was not available, the value provided is an estimate for DMSO. [c] Determined by GC-FID. [d] Determined by ^{1}H NMR spectroscopy.

we postulate that initial oxidation by **2** yields a substrate-based carbon radical that reacted with atmospheric O_2 resulting in auto-oxidation (and thus oxygenated products). The reaction of the carbon-based radical with atmospheric O_2 can also account for the higher-than-expected yields of oxygenated products. Xanthone and fluorenone are 4-electron oxidised products of their parent substrate, triphenylmethanol is a 2-electron oxidised product. Likewise, the greater-than-expected yields of desaturated product from DHA and CHD oxidation can also be attributed to reaction of substrate-based carbon radicals with O_2. In summary, DHA and CHD underwent desaturation upon reaction with **2** (as is favoured by these substrates), while xanthene, fluorene, and triphenylmethane were oxygenated after reaction with **2**. The obtained products indicate that all substrates were oxidised by **2** through an initial PCET oxidation event, followed by reaction with atmospheric oxygen.

To assess the catalytic appositeness of **2**, we added additional oxidant to the post-reaction mixture (Figure 3). Upon depletion of **2** in the presence of xanthene (Figure 3) or CHD (Figure S16), addition of (Phenox)$SbCl_6$ yielded **2** again, as shown by an increase of the features at $\lambda = 657$, 900 nm. Upon regeneration of **2**, monitoring the absorbance at $\lambda = 657$ nm showed the yield was approximately 80 % of that previously obtained in the first oxidation (Figure S16). Furthermore, new features in the near-IR region were apparent, that are assigned to an *iso*-porphyrin decay product below. The newly formed **2** then reacted with the excess of substrate already present in the reaction mixture. Further equivalents of oxidant were added, showing that **2** could be regenerated again over several cycles. This regeneration effect was also found with DHA. This observation is interesting because it demonstrates that a porphyrin-π-cation radical complex is capable of facilitating catalytic hydrocarbon oxidation and oxygenation under aerobic conditions. It also demonstrates that while the porphyrin ring system appears to be involved in the PCET oxidation, it remains somewhat stable to multiple redox/HAT cycles.

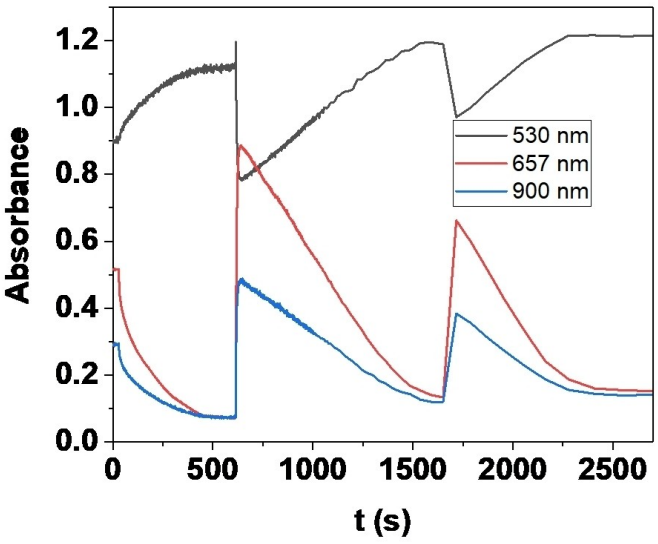

Figure 3. Time trace of the reaction of **2** with xanthene (500 equiv) monitored by electronic absorption spectroscopy (black trace: $\lambda = 530$ nm, red trace: $\lambda = 657$ nm, blue trace: $\lambda = 900$ nm). Oxidant added at $t = 0$ s, 600 s, and 1700 s.

Mechanistic Insight

We reacted **2** with D_2-xanthene to explore any kinetic isotope effects (KIEs). A KIE value of 1.5 was obtained (Figure S17), which is quite low when compared to values obtained for other high-valent oxidants, and is outside the classical range (2–7).[18] In those cases where KIE > 2, a mechanism in which proton transfer (PT) or PCET was rate-determining was normally ascribed. Here, we tentatively conclude that PT or PCET was rate-limiting, acknowledging that the KIE is lower than usual for such reactions.

We noted that substrates with stronger C–H bonds reacted slower than those with weaker C–H bonds, indicating a relationship between the rate of oxidation and substrate C–H bond dissociation free energy ($BDFE_{C-H}$) values. The conversion of the k_2 values obtained for each substrate into the Gibbs free energies of activation ($\Delta G^{\ddagger}$) was performed using the Arrhenius equation. A plot of the $\Delta G^{\ddagger}$ values against the $BDFE_{C-H}$ for each substrate, also known as a Bell–Evans–Polanyi plot,[19] showed a correlation that we have concluded was linear (Figure 4). When a linear trend line was fit ($R^2 = 0.92$), a slope of 0.40 was determined (Figure S18). This value lies within the range reported for oxidants that follow concerted PCET mechanisms (0.15–0.7), such as concerted proton and electron transfer (CPET, proton and electron moving synchronously to different locations) or hydrogen atom transfer (HAT). We then evaluated the Marcus plot, where the oxidation potential of the substrate was plotted against $\log(k_2)$ (Figure S19). Again, the trend was tentatively assessed as being linear ($R^2 = 0.64$), with a small slope (−0.2). In Marcus analyses, a slope closer to 0 (thus a small slope value) has been ascribed

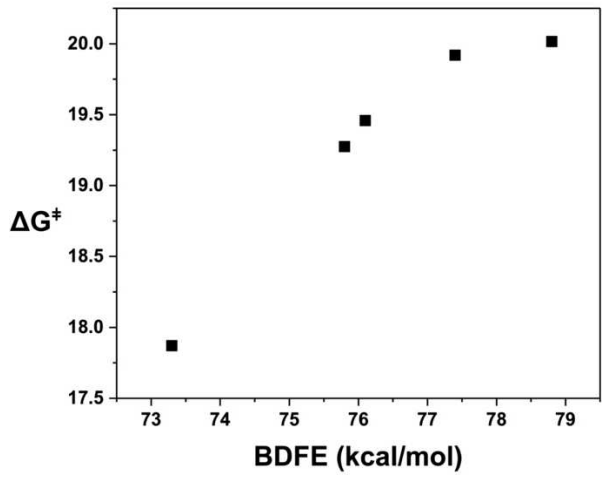

Figure 4. Plot of $\Delta G^{\ddagger}$ against the $BDFE_{C-H}$ of the substrates. The $\Delta G^{\ddagger}$ values were determined from the calculated k_2 via the Arrhenius equation.

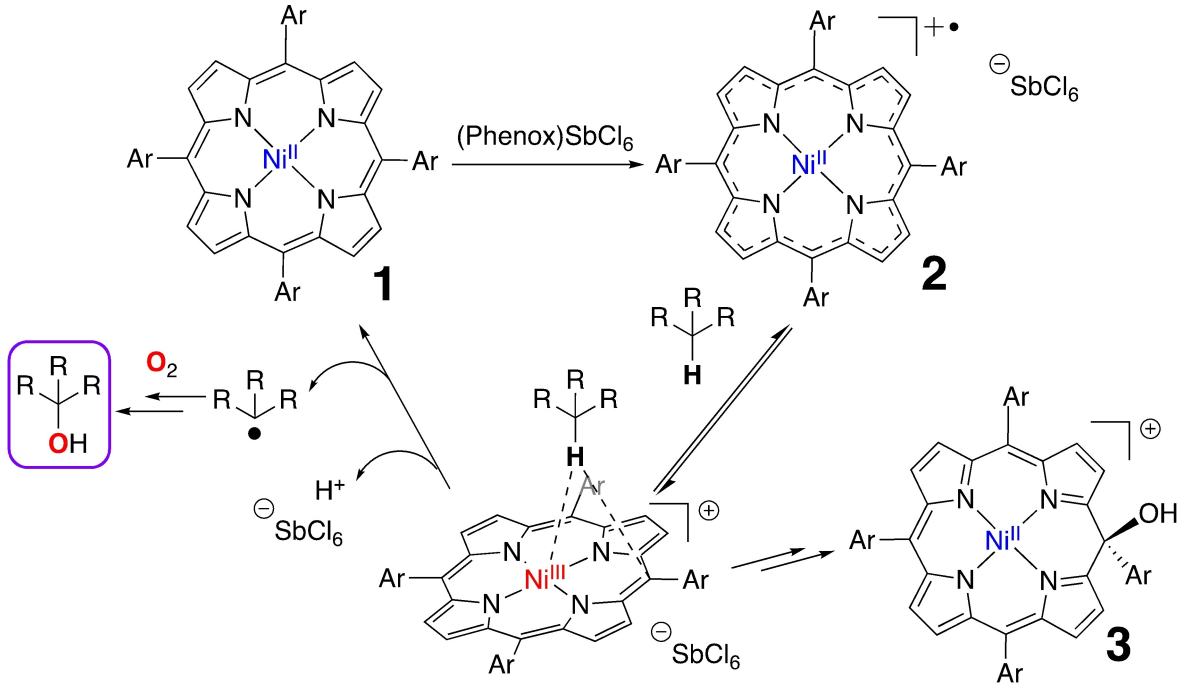

Scheme 2. Postulated mechanism of hydrocarbon oxidative activation by **2**.

to a concerted PCET mechanism, higher values closer to −0.50 to −1.00 suggest that either electron-transfer (ET) or PT was rate limiting.[5e,g,20] Moreover, a plot of the pK_a of the substrates against the log(k_2) showed no correlation (Figure S17).[21] With these combined plots, we tentatively conclude that **2** oxidised hydrocarbons through a concerted PCET mechanism, either CPET or HAT.

Activation parameters were determined by Eyring analysis for the reaction of **2** with xanthene (Figure S20). The activation enthalpy was determined to be $\Delta H^{\ddagger}$ = 8.7 kcal mol^{-1}, and the activation entropy value was determined to be $\Delta S^{\ddagger}$ = −37.5 cal mol^{-1} K^{-1}. The large, negative $\Delta S^{\ddagger}$ is consistent with a metal-based oxidant performing a bimolecular PCET oxidation, due to the higher contribution from vibrational entropy during the reduction of the ligated-metal centre compared to reactions involving organic radicals.[22] The entropic value is therefore suggestive of a metal-involved PCET oxidation.

To gain more insight into the mechanism of hydrocarbon oxidation by **2**, we monitored the reaction of **2** with DHA by EPR (Figure 2): in the absence of substrate, the signal observed was centred at g = 2.00. Upon addition of DHA, the EPR spectrum displayed an additional rhombic signal with g_x = 2.30, g_y = 2.23 and g_z = 2.07. The average g-value g_{av} = 2.20 *and* signal rhombicity, suggested the localisation of the unpaired spin on the metal center, namely a square-planar d^7 Ni^{III} species.[24] The original EPR signal attributed to **2** (g = 2.00) was also present. As the reaction between **2** and DHA proceeded, the intensity of both signals diminished, suggesting that consumption of the inorganic and organic radicals occurred contemporaneously. Analysis of the same reaction by electronic absorption spectroscopy did not provide any insight into the nature of the species associated with the rhombic EPR signal (Figure S9). The EPR spectrum at the end of the reaction was silent, with both the isotropic and rhombic signals consumed, indicating the formation of a formally Ni^{II} species.

Valence tautomerism exists for Ni^{II}-porphyrin-π-cation radical species and is influenced by several factors such as solvent, temperature, porphyrin planarity, and complexation with an external ligand.[12,25] Sometimes the coexistence of both the Ni^{II}-π-cation radical and the Ni^{III} tautomer in solution is possible. The obtained rhombic EPR signal (for **2** in the presence of substrate) was similar to that reported for [Ni^{II}(OEP$^{\bullet+}$)] in the presence of imidazole or pyridine. The signal at g = 2.00 assigned to [Ni^{II}(OEP$^{\bullet+}$)] was converted into an axial signal with g_{av} = 2.13 typical of a Ni^{III} species, once the imidazole or pyridine was coordinated. We postulate that the addition of substrate to **2** induced valence tautomerism, although not through coordination as observed for [Ni^{II}(OEP$^{\bullet+}$)]. To further probe this, we recorded an EPR spectrum of **2** in the presence of an excess of the oxidized product, anthracene (Figure S21). We observed only the g = 2.00 signal, suggesting that the Ni^{III} species was formed only prior to the oxidation event *in the presence of the substrate, not the product.* When **2** was generated with WCl_6, the addition of DHA (500 equiv) resulted in the same two co-existing signals (Figure S22). This result supports the conclusion that an equilibrium between the two tautomers [Ni^{III}(T(MeO)PP)] and [Ni^{II}(T(MeO)PP$^{\bullet+}$)] was induced when the substrate was added to **2** *and* that the sacrificial oxidant (Phenox)$SbCl_6$ or WCl_6 was not responsible for the new rhombic signal.

An analysis of the optical absorption traces obtained at the end of the reaction of **2** with DHA showed features belonging to **1** *and* new features that can be attributed to

porphyrinic species *dissimilar* to those of **1** and **2** (Figure S9). We observed the $\lambda = 530$ nm band attributed to **1** as well as a split in the Soret band alongside the appearance of two features in the near-IR region ($\lambda = 860$, 980 nm). The latter characteristics (split Soret, near-IR bands) are typical of an *iso*-porphyrin complex.[23] The *iso*-porphyrin electronic absorption signals were observed for all substrates except xanthene, which reacted at the highest rate with **2** (Figures S11–S14). In all cases, the yield of the *iso*-porphyrin appeared to be low. Based on the extinction coefficients ($\varepsilon = 1100$–$14\,000\ M^{-1}cm^{-1}$) for the near-IR bands of a closely related *iso*-porphyrin complex,[23] the yield was approximated at a maximum of approximately 20 % with respect to the initial [**1**]. This yield accounts for the "missing" 20 % of **2** when additional oxidant was added to the **2**+DHA reaction mixture (yield of **2** ca. 80 %, Figures 3, S15), suggesting that the *iso*-porphyrin does *not* get re-oxidised upon addition of further oxidant.

^{1}H NMR analysis of the post-reaction mixture from the reaction of **2** with DHA (25 equiv) showed new signals alongside those attributable to **1** (Figure S10). An up-field shift of the resonances in the aromatic region (6.5–8.5 ppm), together with a shift and splitting of the singlet of the $-OCH_3$ group ($\delta = 4.05$ ppm for **1**; $\delta = 4.02$, 4.07 and 4.09 ppm for the new species) was observed. This is indicative of an acquired chemical inequivalence for the protons in the $-OCH_3$ group on the methoxyphenyl *meso*-substituents, which would be observed with the formation of a quaternary *meso*-carbon typical of an *iso*-porphyrin. The post-reaction mixture EPR spectrum was silent, indicating that all radical species had been consumed and the final product likely contained a Ni^{II} ion (Figure 2). Positive mode ESI-MS of the post-reaction mixture of the reaction between **2** and DHA (Figure S23) showed a peak at $m/z = 807.2124$, consistent with the $[Ni(T(MeO)PP)+O+H]^+$ ion. We attribute this signal to a hydroxylated Ni^{II}-*iso*-porphyrin (defined as **3**, Scheme 2, expected $m/z = 807.2160$). Importantly, this mass peak was not observed when the reaction was carried out under anaerobic conditions, nor was it present in the mass spectrum of **2** generated under aerobic conditions (Figures S7, S24). **3** was not observed in the natural decay of **2**. Interestingly, **3** only formed when the reaction between **2** and substrate was slow (**3** was not observed for xanthene oxidation). Our combined observations suggest that the *iso*-porphyrin **3** in the post-reaction mixture is a hydroxylated side-product from a reaction between **2**, substrate, and a reactive oxygen species generated in situ. We surmise that **3** forms from the same auto-oxidation processes that yielded hydroxylated hydrocarbons.

With the elements collected so far, we propose a reaction mechanism for the oxidation of hydrocarbons by **2** (Scheme 2): **2** interacted with substrate which induced the valence tautomerism of **2**. This yielded an adduct which can be formalized as a substrate/Ni^{III} entity as indicated by EPR. A carbon-centred radical was generated and **1** was reformed, as evidenced by post-reaction electronic absorption spectroscopy. The proton acceptor is likely the counterion from the (Phenox)$SbCl_6$ oxidant ($^-SbCl_6$). Substrate oxidation would thus be expected to return **1** through electron transfer to **2**, which is consistent with the regeneration of **2** upon addition of oxidant to the post-reaction mixtures, albeit in lower yields. The lower yields of **2** upon iterative regeneration can be ascribed to a side reaction yielding *iso*-porphyrin **3**.

The mechanistic analysis suggests that the substrate oxidation occurred through a concerted PCET mechanism, either CPET or HAT. The electron appears to return to the porphyrin, while the proton is postulated to associate with the $^-SbCl_6$ anion. This is thus an example of CPET rather than HAT, because the proton and electron move synchronously, but to different locations.[26] For DHA and CHD, the substrate derived carbon-centred radical is then postulated either to react further with another molecule of **2** or atmospheric O_2 to yield the desaturated products anthracene and benzene, respectively. For xanthene, fluorene and triphenylmethane, the formed carbon-centred radical is postulated to react with atmospheric O_2 resulting in auto-oxidation to yield the identified oxygenated products (in greater than expected yields). The same auto-oxidation process is likely the source of the oxygen atom in the hydroxylated *iso*-porphyrin **3**.

Conclusion

We observed that porphyrin-π-cation complex **2** reacted with a pool of hydrocarbon substrates with $BDFE_{C-H}$ ranging from 73 to 79 kcal mol^{-1}, yielding desaturated or oxygenated hydrocarbon products. A kinetic analysis led us to postulate that the porphyrin-π-cation radical species oxidised substrates through a concerted PCET mechanism, namely CPET, where (simultaneously) the electron was transferred to the porphyrin ring and the proton departed with a free anion, $^-SbCl_6$. We believe that these insights are important because they highlight the potential role and mechanistic features of porphyrin-π-cation radicals as hydrocarbon oxidants, demonstrating that porphyrin ligand non-innocence should be considered in assessing the mechanisms of PCET reactivity. Furthermore, we show that oxidation catalyst design can focus on simple ligand frameworks to access entities capable of breaking C–H bonds without the requirement for anionic proton-accepting ancillary ligands.

Acknowledgements

This publication has emanated from research supported by the Irish Research Council under grant number IRCLA/2022/2957 and the European Research Council (ERC-2015-STG-678202). Research in the McDonald lab is supported in part by a research grant from Science Foundation Ireland (SFI/15/RS-URF/3307). We thank Prof. Robert Barklie for training on and use of an EPR spectrometer. Open Access funding provided by IReL.

Conflict of Interest

The authors declare no conflict of interest.

Data Availability Statement

The data that support the findings of this study are available from the corresponding author upon reasonable request.

Keywords: Bioinorganic Chemistry · Heme · High-Valent Oxidants · Oxidation Catalysis · Radicals

[1] a) J. Barber, *Bioelectrochemistry* **2002**, *55*, 135–138; b) H. Ishikita, B. Loll, J. Biesiadka, W. Saenger, E.-W. Knapp, *Biochemistry* **2005**, *44*, 4118–4124; c) J. T. Groves in *Cytochrome P450: Structure, Mechanism, and Biochemistry*, 3rd ed. (Ed.: P. R. Ortiz de Montellano), Kluwer Academic/Plenum Publishers, New York, **2005**, pp. 1–43; d) J. Barber, *Chem. Soc. Rev.* **2009**, *38*, 185–196; e) M. T. Green, *Curr. Opin. Chem. Biol.* **2009**, *13*, 84–88; f) J. M. Kargul, J. Barber, *RSC Energy and Environment Series* **2012**, *1*, 107–142; g) J. T. Groves, *Nat. Chem.* **2014**, *6*, 89–91; h) X. Huang, J. T. Groves, *Chem. Rev.* **2018**, *118*, 2491–2553.

[2] a) J. Rittle, M. T. Green, *Science* **2010**, *330*, 933–937; b) T. H. Yosca, J. Rittle, C. M. Krest, E. L. Onderko, a. Silakov, J. C. Calixto, R. K. Behan, M. T. Green, *Science* **2013**, *342*, 825–829.

[3] J. Barber, M. D. Archer, *J. Photochem. Photobiol. A* **2001**, *142*, 97–106.

[4] a) B. Meunier, *Chem. Rev.* **1992**, *92*, 1411–1456; b) H. Fujii, *Coord. Chem. Rev.* **2002**, *226*, 51–60; c) T. M. Makris, I. G. Denisov, S. G. Sligar, *Biochem. Soc. Trans.* **2003**, *31*, 516–519; d) C. Pavan, J. Legros, C. Bolm, *Adv. Synth. Catal.* **2005**, *347*, 703–705; e) F. P. Guengerich, *ACS Catal.* **2018**, *8*, 10964–10976; f) Y. Ishimizu, Z. Ma, M. Hada, H. Fujii, *J. Biol. Inorg. Chem.* **2019**, *24*, 483–494.

[5] a) E. Kogut, H. L. Wiencko, L. Zhang, D. E. Cordeau, T. H. Warren, *J. Am. Chem. Soc.* **2005**, *127*, 11248–11249; b) C. M. Thomas, N. P. Mankad, J. C. Peters, *J. Am. Chem. Soc.* **2006**, *128*, 4956–4957; c) C. T. Saouma, J. C. Peters, *Coord. Chem. Rev.* **2011**, *255*, 920–937; d) P. Pirovano, E. R. Farquhar, M. Swart, A. R. McDonald, *J. Am. Chem. Soc.* **2016**, *138*, 14362–14370; e) P. Mondal, P. Pirovano, A. Das, E. R. Farquhar, A. R. McDonald, *J. Am. Chem. Soc.* **2018**, *140*, 1834–1841; f) P. Pirovano, A. R. McDonald, *Eur. J. Inorg. Chem.* **2018**, 547–560; g) P. Mondal, M. Lovisari, B. Twamley, A. R. McDonald, *Angew. Chem. Int. Ed.* **2020**, *59*, 13044–13050.

[6] A. Takahashi, T. Kurahashi, H. Fujii, *Inorg. Chem.* **2009**, *48*, 2614–2625.

[7] Z.-Y. Wu, S.-Y. Yang, *J. Mol. Struct.* **2019**, *1188*, 244–254.

[8] M. Fang, S. R. Wilson, K. S. Suslick, *J. Am. Chem. Soc.* **2008**, *130*, 1134–1135.

[9] a) P. J. Chmielewski, L. Latos-Grażyński, *Inorg. Chem.* **1997**, *36*, 840–845; b) H. M. Ahn, J. M. Bae, M. J. Kim, K. H. Bok, H. Y. Jeong, S. J. Lee, C. Kim, *Chem. Eur. J.* **2017**, *23*, 11969–11976.

[10] a) D. Chang, T. Malinski, A. Ulman, K. M. Kadish, *Inorg. Chem.* **1984**, *23*, 817–824; b) Y. Han, Y. Wu, W. Lai, R. Cao, *Inorg. Chem.* **2015**, *54*, 5604–5613.

[11] N. G. Connelly, W. E. Geiger, *Chem. Rev.* **1996**, *96*, 877–910.

[12] G. S. Nahor, P. Neta, P. Hambright, L. R. Robinson, *J. Phys. Chem.* **1991**, *95*, 4415–4418.

[13] C. E. Schulz, H. Song, Y. J. Lee, J. U. Mondal, K. Mohanrao, C. A. Reed, F. A. Walker, W. R. Scheidt, *J. Am. Chem. Soc.* **1994**, *116*, 7196–7203.

[14] E. T. Shimomura, M. A. Phillippi, H. M. Goff, W. F. Scholz, C. A. Reed, *J. Am. Chem. Soc.* **1981**, *103*, 6778–6780.

[15] J. Seth, V. Palaniappan, D. F. Bocian, *Inorg. Chem.* **1995**, *34*, 2201–2206.

[16] V. N. Pak, D. V. Korol'kov, *Theor. Exp. Chem.* **1973**, *6*, 315–317.

[17] D. Mandal, S. Shaik, *J. Am. Chem. Soc.* **2016**, *138*, 2094–2097.

[18] F. H. Westheimer, *Chem. Rev.* **1961**, *61*, 265–273.

[19] a) J. J. Warren, T. A. Tronic, J. M. Mayer, *Chem. Rev.* **2010**, *110*, 6961–7001; b) J. W. Darcy, B. Koronkiewicz, G. A. Parada, J. M. Mayer, *Acc. Chem. Res.* **2018**, *51*, 2391–2399.

[20] P. Mondal, A. R. McDonald, *Chem. Eur. J.* **2020**, *26*, 10083–10089.

[21] M. K. Goetz, J. S. Anderson, *J. Am. Chem. Soc.* **2019**, *141*, 4051–4062.

[22] a) E. A. Mader, E. R. Davidson, J. M. Mayer, *J. Am. Chem. Soc.* **2007**, *129*, 5153–5166; b) E. A. Mader, V. W. Manner, T. F. Markle, A. Wu, J. A. Franz, J. M. Mayer, *J. Am. Chem. Soc.* **2009**, *131*, 4335–4345.

[23] a) D. Dolphin, R. H. Felton, D. C. Borg, J. Fajer, *J. Am. Chem. Soc.* **1970**, *92*, 743–745; b) R. Gericke, L. M. Doyle, E. R. Farquhar, A. R. McDonald, *Inorg. Chem.* **2020**, *59*, 13952–13961.

[24] a) R. I. Haines, A. McAuley, *Coord. Chem. Rev.* **1981**, *39*, 77–119; b) P. Pirovano, B. Twamley, A. R. McDonald, *Chem. Eur. J.* **2018**, *24*, 5238–5245.

[25] a) M. W. Renner, K. M. Barkigia, Y. Zhang, C. J. Medforth, K. M. Smith, J. Fajer, *J. Am. Chem. Soc.* **1994**, *116*, 8582–8592; b) K. M. Barkigia, M. W. Renner, J. Fajer, *J. Phys. Chem. B* **1997**, *101*, 8398–8401; c) M. W. Renner, J. Fajer, *J. Biol. Inorg. Chem.* **2001**, *6*, 823–830; d) M. W. Renner, K. M. Barkigia, D. Melamed, J.-P. Gisselbrecht, N. Y. Nelson, K. M. Smith, J. Fajer, *Res. Chem. Intermed.* **2002**, *28*, 741–759; e) K. M. Kadish, M. Lin, E. V. Caemelbecke, G. De Stefano, C. J. Medforth, D. J. Nurco, N. Y. Nelson, B. Krattinger, C. M. Muzzi, L. Jaquinod, Y. Xu, D. C. Shyr, K. M. Smith, J. A. Shelnutt, *Inorg. Chem.* **2002**, *41*, 6673–6687.

[26] W. D. Morris, J. M. Mayer, *J. Am. Chem. Soc.* **2017**, *139*, 10312–10319.

Manuscript received: March 1, 2023
Accepted manuscript online: June 6, 2023
Version of record online: June 27, 2023